Japanese Journal of Applied Physics REGULAR PAPER

# Comparative study of (0001) and (11$\bar{2}$2) InGaN based light emitting diodes

Markus Pristovsek[1], Colin J. Humphreys[1], Sebastian Bauer[2], Manuel Knab[2], Klaus Thonke[2], Grzegorz Kozlowski[3], Donagh O'Mahony[3], Pleun Maaskant[3], and Brian Corbett[3]

[1] *Department of Materials Science and Metallurgy, University of Cambridge, 27 Charles Babbage Road, Cambridge, CB3 0FS, UK*
[2] *Universität Ulm, Institute of Quantum Matter, Semiconductor Physics Group, D-89069 Ulm, Germany*
[3] *Tyndall National Institute, Lee Maltings, Cork, T12 R5CP, Ireland*

We have systematically investigated the doping of (11$\bar{2}$2) with Si and Mg by metal-organic vapour phase epitaxy for light emitting diodes (LEDs). By Si doping of GaN we reached electron concentrations close to $10^{20}$ cm$^{-3}$, but the topography degrades above mid $10^{19}$ cm$^{-3}$. By Mg doping we reached hole concentrations close to $5\times10^{17}$ cm$^{-3}$, using Mg partial pressures about 3× higher than those for (0001). Exceeding the maximum Mg partial pressure led to a quick degradation of the sample. Low resistivities as well as high hole concentrations required a growth temperature of 900°C or higher. At optimised conditions the electrical properties as well as the photoluminescence of (11$\bar{2}$2) p-GaN were similar to (0001) p-GaN. The best ohmic p-contacts were achieved by NiAg metallisation. A single quantum well LED emitting at 465 nm was realised on (0001) and (11$\bar{2}$2). Droop (sub-linear increase of the light output power) occurred at much higher current densities on (11$\bar{2}$2). However, the light output of the (0001) LED was higher than that of (11$\bar{2}$2) until deep in the droop regime. Our LEDs as well as those in the literature indicate a reduction in efficiency from (0001) over semi-polar to non-polar orientations. We propose that reduced fields open a loss channel for carriers.

## 1. Introduction

The efficiency of InGaN based light emitting diodes drops from typically 80% in the blue spectral range to below 10% for yellow green. A common explanation is the increasing vertical separation between electron and hole wave functions in the quantum well (QW). Semi-polar and non-polar orientations are currently under close investigation, since these have strongly reduced or even eliminated the piezo-electric polarisation fields. The then enlarged overlap between electron and hole wave functions should increase the radiative recombination and shorten radiative carrier lifetimes.[1,2] Since fast recombination reduces the carrier density in the QW, the sub-linear increase of light output at high currents (droop) is reduced, too.[3,4]

An especially promising semi-polar orientation is (11$\bar{2}$2), because it is a stable surface during growth. Several groups demonstrated the fabrication of low defect density templates on patterned r-plane sapphire of up to 4" size.[5] There have been several reports on (11$\bar{2}$2) LEDs grown in this orientation.[3,4,6–9] Most of them had rather high forward voltages in excess of 5 V at 20 mA.[6–9] This may be related to a non-optimised p-GaN layer, since the Mg uptake is much lower for (11$\bar{2}$2) than for any other orientation.[10] Therefore, in the first part of this study, we focussed on doping and contacts of (11$\bar{2}$2) GaN. The obtained results were used to produce LEDs. The LEDs were directly compared to (0001), which so far has been conducted only once on a different semi-polar orieation, the (10$\bar{1}$1).[4]

## 2. Experimental procedure

The samples were grown in an Aixtron 6x2-inch close-coupled showerhead reactor. To avoid memory effects, the reactor was baked after each run. We first deposited an AlN nucleation layer, starting with annealing the substrate in $H_2$, followed by 20 nm AlN deposited at 1040°C, and 80 nm AlN at 1100°C. On these about 500 nm graded AlGaN were deposited by ramping the temperature to 1020°C while increasing the trimethylgallium (TMGa) flow rate and then a short constant deposition. This 20% Al-containing layer was annealed for 5 min at 1050°C. Finally, a 500 nm GaN buffer was grown with a high V/III ratio and a high growth rate (≈ 3.5 $\mu$m/h). This results in very smooth, semi-insulating templates with about $10^9$ cm$^{-2}$ dislocations and mid $10^5$ cm$^{-1}$ stacking faults.[11]

The n-doped GaN layer had a typical thickness of 2 $\mu$m (35 min growth time). We used $SiH_4$ diluted to 500 ppm in hydrogen and the same conditions as those for buffer growth. The p-doped GaN layer was grown for 1 h at 15 kPa $H_2$ with a total flow rate of 30 l/min. The $NH_3$ flow rate was 10 l/min, the V/III ratio ≈ 5000, and the Bis(cyclopentadienyl)magnesium ($Cp_2Mg$) flow rate was varied. $Cp_2Mg$ was introduced 60 s before introducing TMGa. The TMGa partial pressure was fixed at 0.3 Pa, leading to a growth rate of 800 nm/h. The p-doped GaN layer was capped with a 10 nm $p^{++}$ contact layer grown at half of the growth rate of the p-GaN. The samples were annealed afterwards in the reactor under $N_2$ for 20 min. at 800-850°C.

The LEDs were grown on patterned templates with low defect densities,[5] or on 0.3° off oriented (0001) sapphire. Because of the much lower Mg incorporation of (11$\bar{2}$2) and the different emission wavelengths of QWs with the same In content on (0001) and (11$\bar{2}$2), each LED was grown separately in subsequent runs. We slightly increased the temperatures during the QW growth and used a much lower $Cp_2Mg$ flow rate on (0001) than on (11$\bar{2}$2). Before and after the QWs we deposited a 10 nm undoped GaN layer under barrier conditions. The QWs were grown at temperatures lower than those of the barriers, with an additional GaN capping before raising temperature, in the so-called quasi two temperature scheme.

The details of the QWs are reported elsewhere.[12]

Carrier concentration was determined using a van der Pauw-type Hall measurement setup at room temperature using a 900 mT magnet. The samples were cleaved into $7 \times 7\,\mathrm{mm}^2$ pieces and contacted by indium wire. For each sample three to five pieces were measured about three times. The error bars in the figures indicate the standard deviation. Some samples were measured by a C(V) setup using mercury contacts, and one sample was profiled by secondary ion mass spectroscopy (SIMS) at RTG-Mikroanalyse Berlin, Germany.

Room temperature photoluminescence (PL) was measured with an Accent RPM2000 PLM mapper with excitation by a pulsed Q-switched laser at 266 nm with a power of ≈2.2 mW on the sample. Low temperature PL (approximately 6-10 K) was measured with a cw 325 nm HeCd laser at lower excitation power densities.

Devices were processed with a mask containing circular transfer length measurement (cTLM) patterns as well as circular LEDs. Electroluminescence was measured on-chip on LEDs with diameters between 40 and 460 $\mu$m with DC up to 10-50 $\mathrm{A/cm}^{-2}$ and then pulsed with less than 5% duty cycle. Light was either collected from the front via a fibre through a microscope or from the back using a large area photo diode.

## 3. Results and discussion

### 3.1 Doping and contacts

We realised very high electron concentrations close to $10^{20}\,\mathrm{cm}^{-3}$ for Si doped $(11\bar{2}2)$ GaN [Fig. 1 (a)]. The mobility linearly decreased from $150\,\mathrm{cm}^2\mathrm{V}^{-1}\mathrm{s}^{-1}$ at $n = 2 \times 10^{19}\,\mathrm{cm}^{-3}$ to $70\,\mathrm{cm}^2\mathrm{V}^{-1}\mathrm{s}^{-1}$ at $n = 9 \times 10^{19}\,\mathrm{cm}^{-3}$ [Fig. 1 (b)]. These values are higher than previously reported ones for (0001) GaN[13–15] or smooth $(11\bar{2}0)$ GaN.[16,17] Only for $(11\bar{2}0)$ GaN doped with Si there exists a report of $n = 8.9 \times 10^{19}\,\mathrm{cm}^{-3}$ and $\mu = 100\,\mathrm{cm}^2\mathrm{V}^{-1}\mathrm{s}^{-1}$.[18] Our mobility also compares well with the values reported for (0001) GaN of $\mu = 150\,\mathrm{cm}^2\mathrm{V}^{-1}\mathrm{s}^{-1}$ at $n = 10^{19}\,\mathrm{cm}^{-3}$.[14,15]

On $(11\bar{2}2)$ GaN a strong formation of chevrons sets on when the $SiH_4$ to TMGa ratio exceeds 1/1000 [images in Fig. 1 (a)]. This is most likely due to the local passivation by SiN, which masks the surface and locally prevents further growth. This effect of $SiH_4$ has been deliberately used to reduce defects by inducing three dimensional growth.[11,19] A similar effect of $SiH_4$ was reported on the topography of $(11\bar{2}0)$ GaN.[18] Overall, the incorporation of Si on $(11\bar{2}2)$ behaves similarly to that on $(11\bar{2}0)$.

It was previously reported that the $(11\bar{2}2)$ surface needs a 2-3 times higher $Cp_2Mg$ flow rate than the (0001) surface to obtain a similar Mg incorporation.[10,20,21] Hence, first we targeted the $Cp_2Mg$ flow rate. When a certain $Cp_2Mg$ flow rate was exceeded, we observed many dark spots in the optical microscope [Fig. 2], and the Fabry-Pérot oscillations vanished. These dark spots originate from tilted pyramidal inversion domains (PIDs), which have been observed on (0001).[22] Their appearance is a good indication of exceeding the maximum allowable $Cp_2Mg$ flow rate. However, this contradicts a recent report that found no overdoping effects in semi-

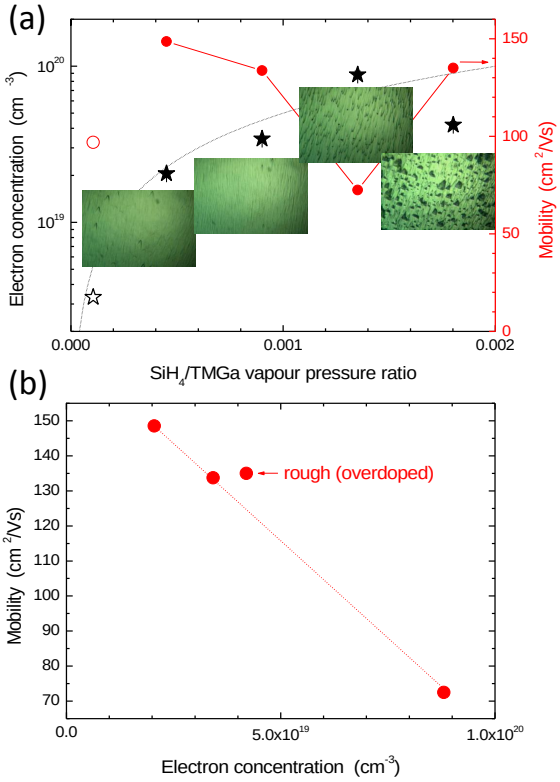


**Fig. 1.** (Color online) (a) Electron concentration and mobility as a function of $Si_4$ to vapour pressure ratio at constant TMGa flow rate. The dotted line corresponds to a linear increase in carrier concentration. The optical microscopy images are $80 \times 120\,\mu m^2$. The open symbols indicate doping with a 50 ppm dilution $SiH_4$ line on a more defective GaN template. (b) Mobility as function of carrier concentration.

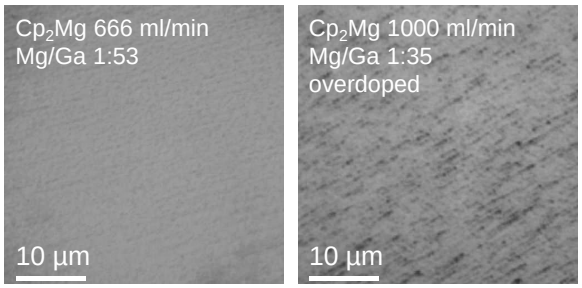


**Fig. 2.** $40 \times 40\,\mu m^2$ bright field optical microscopy images of a p-doped layer at a $Cp_2Mg$ flow rate of 666 ml/min (left) and an overdoped layer at 1000 ml/min (right). The $Cp_2Mg$ to TMGa vapour pressure ratios are given in the figure.

polar GaN:Mg.[21]

We also tried Mg doping using $N_2$ carrier gas. However, the resulting $(11\bar{2}2)$ Mg:GaN was highly insultating. This underlines the difference in incorporation mechanism between $(11\bar{2}2)$ and (0001), as already indicated by the higher required Mg flow rates on $(11\bar{2}2)$.

Overall, two parameters were found to be important: surface growth temperature and $Cp_2Mg$ flow (Fig. 3). The maximum hole concentration achieved at room temperature was $p = 4.6 \times 10^{17}\,\mathrm{cm}^{-3}$ at a $Cp_2Mg$ flow of 850 ml/min, i.e. a Mg/Ga ratio of 50. Overdoping already

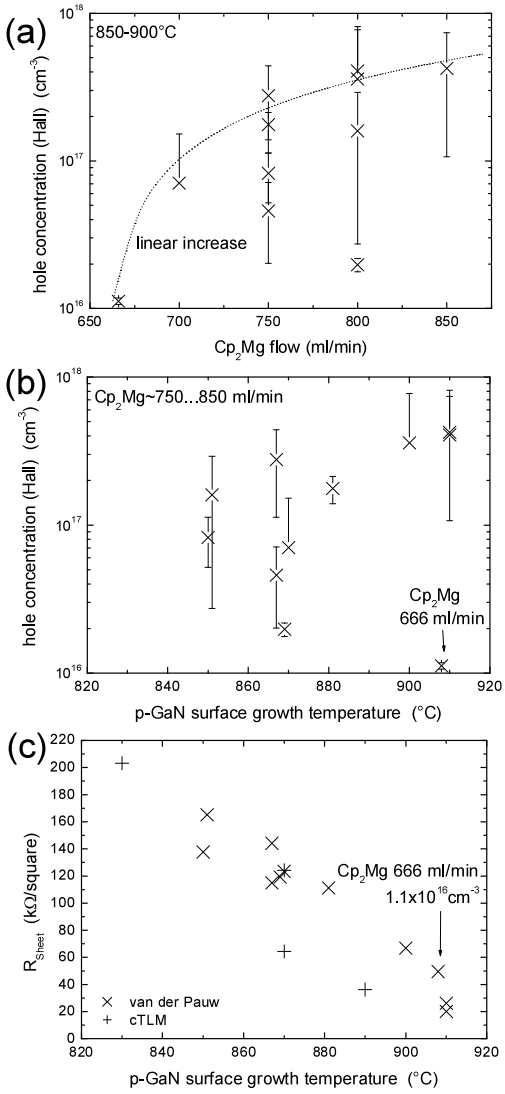


**Fig. 3.** (a) Hole concentration as a function of $Cp_2Mg$ flow rate. The dotted line indicates a linear increase. (b) The same data plotted over the growth temperature show an increased hole concentration at higher growth temperatures. (c) Increasing the growth temperature also decreases the sheet resistance as measured by van der Pauw (×) and cTLM (+) on processed LEDs wafers.

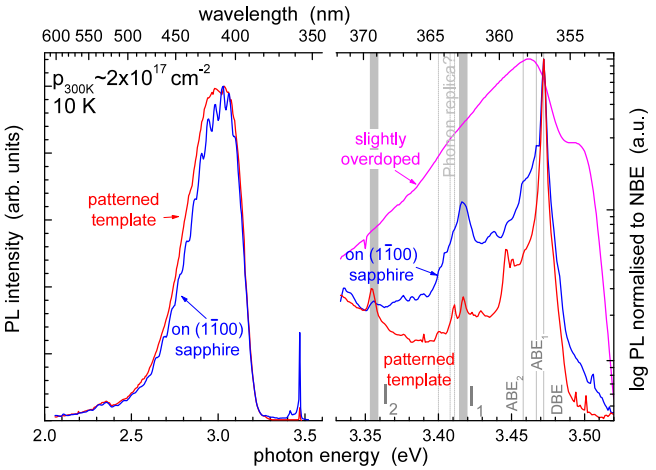


**Fig. 4.** (Color online) Left half shows the typical low temperature PL on a hetero-epitaxial sample on (1$\bar{1}$00) sapphire (with $\approx 10^5\,\mathrm{cm}^{-1}$ BSFs) and on a patterned template (with very low BSF density) both with $p = 2 - 3 \times 10^{17}\,\mathrm{cm}^{-2}$ holes. The PL signal is dominated by the Mg-related blue PL (left). The near band edge is plotted also on the logarithmic scale on the right, together with the PL signal of a slightly overdoped region on the same hetero-epitaxial sample. The vertical lines indicate the energy position of DBE, $ABE_1$, and $ABE_2$ transition,[24] and the dotted lines the respective phonon replicas. Thick grey areas indicate the position of $I_1$ BSF and $I_2$ BSF.[25]

starts at 900 ml/min, and the density of PIDs increased when the $Cp_2Mg$ flow rate was increased further (Fig. 2 right). Hall measurements of overdoped layers showed alternating conductivity with very low mobilities.

$Cp_2Mg$ flow rate linearly correlated with hole concentration [dotted line in Fig. 3 (a)]. The offset of 650 ml/min is due to compensating donors, especially oxygen.[20] A $Cp_2Mg$ flow rate of 700 ml/min corresponded to $6 \times 10^{19}\,\mathrm{cm}^{-3}$ Mg atoms, as determined by SIMS. Mercury contact C(V) measurements of samples grown at a $Cp_2Mg$ flow rate of 750 ml/min showed $N_A \approx 1.5 \times 10^{19}\,\mathrm{cm}^{-3}$ acceptor concentration. Both numbers correspond well to the measured hole concentrations of $4 \times 10^{17}\,\mathrm{cm}^{-3}$.

The variation of growth temperature also affected hole concentration. The highest hole concentrations were only achieved for growth above 900°C [Fig. 3 (b)]. One might speculate that at lower temperatures the Mg may compete with carbon for incorporation, or is partly compensated by carbon. Growth temperatures above 950°C reduced again the hole concentrations, probably due to Mg desorption. Furthermore, long wavelength semi-polar LEDs require growth temperatures as low as possible to avoid the decomposition of the underlying InGaN QWs. So we focussed on the low growth temperatures.

The mobilities was approximately $5\,\mathrm{cm}^2\mathrm{V}^{-1}\mathrm{s}^{-1}$ for mid $10^{17}\,\mathrm{cm}^{-2}$, which is also typical for MOVPE-grown (0001) GaN:Mg. When using MBE about three times higher values were reported for (0001) and (10$\bar{1}$0).[23] Similar to hole concentration, mobilities were independent from defect densities of the GaN templates, which is expected since the Mg concentration exceeds the number of defects by three to five orders of magnitude, and the impurity scattering should dominate over defect scattering.

To examine in more detail the effect of growth temperature independent of hole concentration, we plotted sheet resistance vs. growth temperature in Fig. 3 (c). The sheet resistance reduces by a factor of ten when the growth temperature was increased from 830°C to 910°C. This reduction is likely related to the reduction in the density of point defects such as carbon from TMGa, which partly compensates the Mg, and also enhances scattering. Indeed, the PL spectra of samples grown above 880°C showed an increased near band edge (NBE) intensity.

For samples grown on m-sapphire most PL spectra only show a broad PL band centered around 3.15 eV (395 nm) at 300 K and 410 nm at 10 K (Fig. 4). This band corresponds to the blue PL typical for Mg concentrations close to $10^{20}\,\mathrm{cm}^{-2}$.[26,27] Near the band edge, the PL ratio of donor-bound excitons (DBE) to acceptor-bound excitons (ABE) on (11$\bar{2}$2) is more close to (0001) than that on

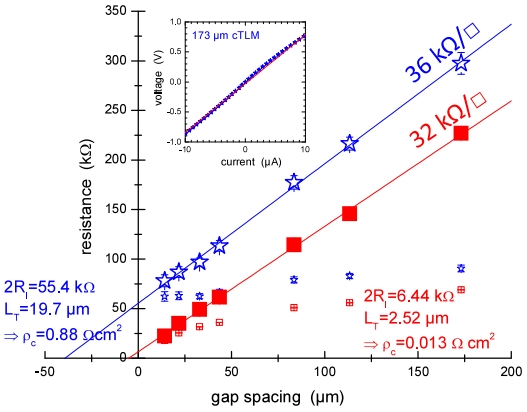


**Fig. 5.** (Color online) cTLM of $(11\bar{2}2)$ ($\star$) and (0001) ($\square$) uncorrected (small) and after correction.[28] The inset shows the I(V) curve of a $(11\bar{2}2)$ sample with Ni/Ag contacts.

$(10\bar{1}0)$, i.e. strong DBE and $ABE_2$ peaks, and only weak $ABE_1$ peaks. [Note however that the $(10\bar{1}0)$ spectra in Ref.[24] were recorded on a sample with only $3\times10^{18}\,\mathrm{cm}^{-2}$ Mg.] There are peaks near an expected phonon replica of DBE and $ABE_2$ on the low defect density patterned substrate. However, this is also the spectral region where the BSF-related PL dominates.[25] Generally, the PL is comparable to that of (0001) GaN:Mg.

For contacts, we deposited on the Mg:GaN a 10 nm thick $p^{++}$ GaN layer at the maximum $Cp_2Mg$ flow rate of 1000 ml/min while the growth rate was reduced to one-third. On such layers various metallisation procedures (Ni/Au, Pd, and Ni/Ag) were tried out. In the end we obtained the best (and most reproducible) results using Ni/Ag, which was moderately annealed. Even though electrical properties of the GaN:Mg on (0001) and $(11\bar{2}2)$ were comparable in Hall measurements, the contact resistance of the $(11\bar{2}2)$ layers were almost ten times higher (Fig. 5). This may bedue to a $p^{++}$ layer with lower amount of Mg compared to (0001) [as also indicated by recent results on $(20\bar{2}1)$[21]]. Another reason could be the much higher tendency of $(11\bar{2}2)$ to incorporate oxygen, i.e. there might be a greater oxygen incorporation (and hence compensation) during the annealing of the contacts. The higher resistance of $(11\bar{2}2)$ contacts is also the reason for the higher voltage drop in our semi-polar LEDs (Fig. 6 b). Nevertheless, the forward voltages at $20\,\mathrm{A/cm}^2$ were still below 4 V.

### 3.2 LED performance

Figure 6 (a) shows the relative external quantum efficiency (EQE) of the simplest LED structure possible, namely a single QW, no electron blocking layers, no InGaN underlayers, and a GaN barrier. Up to $2\,\mathrm{A\,cm}^{-2}$ [peak of (0001) EQE] the ratio of EL is 10:1 between (0001) and $(11\bar{2}2)$. Only deep in the droop regime the EQE of $(11\bar{2}2)$ finally surpasses that of (0001). To exclude effects of the patterning of the sapphire templates on the light extraction, we repeated the measurements with the light collected from the back. The mean intensity ratio was again approximately 10. For additional verification, we measured the same structure on a more

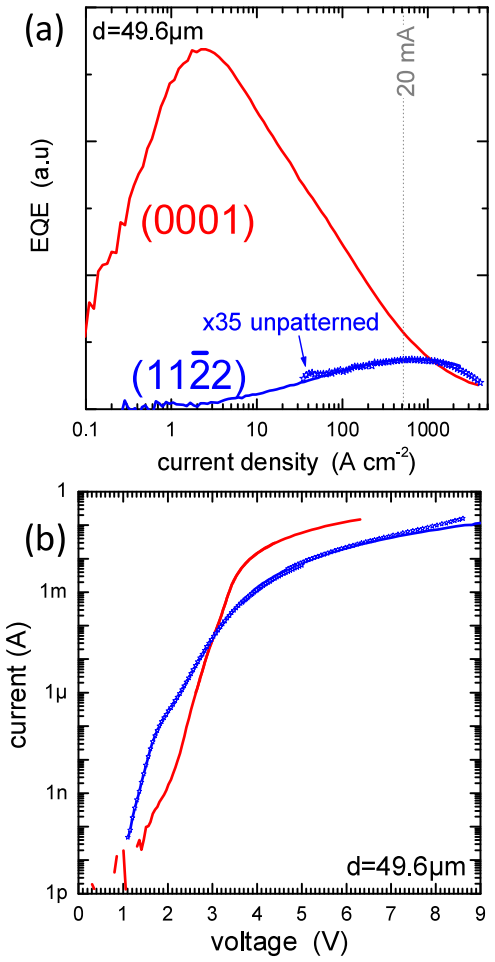


**Fig. 6.** (Color online) EQE curves (a) and I(V) curves (b) for a single QW LED with a diameter of 49.6 $\mu m$ emitting at 465 nm. The stars indicate measurements on a simultaneously grown $(11\bar{2}2)$ LED directly on $(1\bar{1}00)$ sapphire with a much higher BSF density. Thus the EQEs are scaled up on the latter by 35×.

defective $(11\bar{2}2)$ template grown directly on $(1\bar{1}00)$ sapphire. Owing to the higher defect densities, the LED output was further reduced by a factor of 35. Nevertheless, the droop behaviour on both $(11\bar{2}2)$ LEDs was very similar, i.e. onset of droop at much higher currents. A high onset of droop (at least for blue LEDs) for semi-polar was also previously reported for $(11\bar{2}2)$,[3] and $(10\bar{1}1)$.[4]

We fitted EQE(L) curves by the single parameter fitting method from the *ABC* model.[53] The obtained internal quantum efficiencies (IQEs) were between 40-70% for (0001), and 10-50% for $(11\bar{2}2)$ for blue LEDs. On (0001) these IQE ranges seem realistic for a single QW close to a GaN:Mg layer, and the values for $(11\bar{2}2)$ are close to reported PL IQEs.[54,55] Therefore, the lower light output at low currents of the semi-polar LEDs is due to some fundamental processes and not due to light extraction issues.

This is consistent with findings in the literature. Figure 7 shows the highest reported EQEs at 20 mA (with different chips sizes and hence at different current densities). Our values were scaled assuming 50% EQE at 440 nm. At any given wavelength, the highest EQEs have been reported for (0001), followed by semi-polar $(11\bar{2}2)$

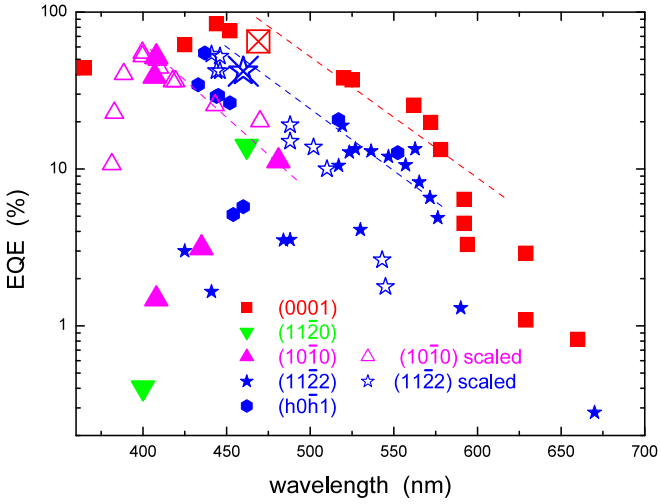


**Fig. 7.** (Color online) Reported EQEs at 20 mA over wavelength for LEDs on (0001),[29–37] non-polar (11$\bar{2}$0)[38,39] and (10$\bar{1}$0)[40–43] and semi-polar (11$\bar{2}$2),[3,4,6,9,44–46] (1$\bar{1}$01),[4,47,48] (20$\bar{2}$1)[46,49] and (30$\bar{3}$1).[50] The open triangles for (10$\bar{1}$0) are data from Ref.[51] scaled to 52% at 400 nm (cf. Ref.[43]) and the open stars for (11$\bar{2}$2) are from[52] scaled to 54% EQE at 441 nm (cf. ref.[48]) and from our own samples measured on the same setup. The open crossed symbols indicate the single QW LEDs for which the peak IQE has been fitted.

and (h0$\bar{h}$1), and the lowest EQE were for non-polar (11$\bar{2}$0) and (10$\bar{1}$0). This is quite surprising, since the wave function overlap increases from polar to non-polar, as demonstrated by shorter radiative lifetimes, e.g. refs.[1] and.[2] However, the trend of the EQE is in agreement with that of PL IQEs, which are lower on semi-polar[54,55] and non-polar.[56]

Figure 7 shows a marked decrease in EQE with increasing wavelengths for semi-polar LEDs as well, despite their lower internal fields. This observation strongly questions the wave function overlap as the only cause of the green gap. Otherwise, the larger wave function overlap for semi-polar LEDs should result in a more gradual reduction. A recent publication[57] suggests that the lower growth temperatures needed for longer wavelengths are associated with lower IQEs on (0001). This effect would be independent of the surface orientation, since the QW growth temperatures of (0001) and (11$\bar{2}$2) are comparable.[12] Further studies are required.

The direct comparison of the L(I) curves between (0001) and semi-polar LEDs [as in Fig. 6 (a)] gives some interesting insight into droop. The semi-polar LEDs had a later onset of droop [Fig. 6 (b)],[3,4] and non-polar LEDs showed almost no droop at all.[41,58] This is usually explained by the greater wave function overlap, which results in a lower carrier density in the active region. Hence, the cubic "Auger" losses occur later in semi-/non-polar LEDs. However, at moderate current densities the EQEs are lower for semi-polar LEDs, and even further reduced for non-polar LEDs, despite a faster recombination, which should result in brighter emission, i.e. higher EQEs. One possible explanation would be that carriers are lost easier from the active region at lower polarisation fields, i.e. a loss channel that becomes more effective at lower internal fields. Indeed, systematically higher injection losses in semipolar LEDs have been observed in a recent study.[59] If this loss of carriers is reduced by the internal fields, then screening of these fields at high currents on (0001) would open the same loss channel, which is already active in semi-polar LEDs and even stronger in non-polar LEDs. As a consequence, non-polar devices do not show much droop (as reported) but would always have a lower EQE, because their loss channel is already fully active at low current densities. If this model is true, at very high current densities the EQEs of non-polar, semi-polar, and polar LEDs would become similar at all wavelengths.

## 4. Conclusions

N-doping with $SiH_4$ works better for (11$\bar{2}$2) than for (0001). Without roughening, electron concentrations close to $5 \times 10^{19}\,\mathrm{cm}^{-2}$ were obtained with a mobility of $130\,\mathrm{cm}^2\mathrm{V}^{-1}\mathrm{s}^{-1}$. For p-doping of (11$\bar{2}$2) GaN, $Cp_2Mg$ flow rate as well as the growth temperature are important. Low resistivity and high hole concentration require growth temperatures between 900°C and 950°C and a threefold higher Mg flow rates than that for (0001). The transition to overdoping and layer degradation is quite sharp. Nevertheless, the electrical properties of optimised (11$\bar{2}$2) and (0001) p-GaN were similar.

Our LED data as well as literature data indicate that the EQEs at longer wavelengths are significantly lower on semi-polar LEDs than on (0001) LEDs. Moreover, semi-polar LEDs show a similar EQE reduction towards longer wavelength as (0001) LEDs (green gap). Hence, a reduced wave function overlap cannot explain the green gap alone.

At high current densities, the EQE of semi-polar LEDs reach those of (0001) LEDs, when they alreadz show a strong droop. We propose that reduced fields in the QW lead to a loss mechanism, such as escape of carriers from the active region and recombination in the doped layers around the active region. In more polar LEDs this loss mechanism only becomes active at higher current densities that shield the internal fields. Therefore, more polar LEDs show more droop.

## Acknowledgment

This work was supported by EU-FP7 ALIGHT No. NMP-2011-280587. The data used to produce the figures can be found under the permanent URL `https://www.repository.cam.ac.uk/handle/1810/253538`.

1) M. Ueda, K. Kojima, M. Funato, Y. Kawakami, Y. Narukawa, and T. Mukai: Appl. Phys. Lett. **89**(21) (2006) 211907.
2) M. Funato and Y. Kawakami: J. Appl. Phys. **103**(9) (2008) 093501.
3) M. Funato, M. Ueda, Y. Kawakami, Y. Narukawa, T. Kosugi, M. Takahashi, and T. Mukai: Jpn. J. Appl. Phys. **45**(7L) (2006) L659.
4) H. Sato, H. Hirasawa, H. Asamizu, N. Fellows, A. Tyagi, M. Saito, K. Fujito, J. S. Speck, S. P. Denbaars, and S. Nakamura: J. Light Visual Environ. **32**(2) (2008) 107.
5) F. Brunner, U. Zeimer, F. Edokama, W. John, D. Prasai, O. Krüger, and M. Weyers: phys. stat. sol. (b) **252**(5) (2015)

1189.
6) H. Sato, R. B. Chung, H. Hirasawa, N. Fellows, H. Masui, F. Wu, M. Saito, K. Fujito, J. S. Speck, S. P. DenBaars, and S. Nakamura: Appl. Phys. Lett. **92**(22) (2008) 221110.
7) T. Hikosaka, T. Tanikawa, Y. Honda, M. Yamaguchi, and N. Sawaki: phys. stat. sol. (c) **5**(6) (2008) 2234.
8) B. Leung, Q. Sun, C. Yerino, Y. Zhang, J. Han, B. H. Kong, H. K. Cho, K.-Y. Liao, and Y.-L. Li: J. Cryst. Growth **341**(1) (2012) 27 .
9) D. S. Kim, S. Lee, D. Young Kim, S. K. Sharma, S.-M. Hwang, and Y. Gon Seo: Appl. Phys. Lett. **103**(2) (2013) 021111.
10) S. C. Cruz, S. Keller, T. E. Mates, U. K. Mishra, and S. P. DenBaars: J. Crystal Growth **311**(15) (2009) 3817 .
11) M. Pristovsek, M. Frentrup, Y. Han, and C. J. Humphreys: phys. stat. sol. (b) **253** (2016) 61.
12) M. Pristovsek, Y. Han, T. Zhu, C. J. Humphreys, D. Tytko, P.-P. Choi, D. Raabe, F. Brunner, and M. Weyers: Semicond. Sci. Technol. **submitted**.
13) S. Nakamura, T. Mukai, and M. Senoh: Jpn. J. Appl. Phys. **31**(9R) (1992) 2883.
14) L. B. Rowland, K. Doverspike, and D. K. Gaskill: Appl. Phys. Lett. **66**(12) (1995) 1495.
15) J. K. Sheu and G. C. Chi: J. Phys.: Condens. Matter **14**(22) (2002) R657.
16) S. Xu, X. Zhou, Y. Hao, L. Yang, J. Zhang, W. Mao, C. Yang, M. Cai, X. Ou, L. Shi, and Y. Cao: Sci. China Tech. Sci. **53**(9) (2010) 2363.
17) K. M. Song, C. Z. Kim, J. M. Kim, D. H. Yoon, S. M. Hwang, and H. Kim: Jpn. J. Appl. Phys. **50**(5R) (2011) 055502.
18) M. Wieneke, H. Witte, K. Lange, M. Feneberg, A. Dadgar, J. Bläsing, R. Goldhahn, and A. Krost: Appl. Phys. Lett. **103**(1) (2013) 012103.
19) J. Jeong, J. Jang, J. Hwang, C. Jung, J. Kim, K. Lee, H. Lim, and O. Nam: J. Cryst. Growth **370**(0) (2013) 114 .
20) F. Scholz, T. Meisch, M. Caliebe, S. Schörner, K. Thonke, L. Kirste, S. Bauer, S. Lazarev, and T. Baumbach: J. Cryst. Growth **405**(0) (2014) 97 .
21) M. Rychetsky, I. L. Koslow, T. Wernicke, J. Rass, V. Hoffmann, M. Weyers, and M. Kneissl: phys. stat sol. (b) **253** (2016) 169.
22) M. Leroux, P. Vennéguès, S. Dalmasso, M. Benaissa, E. Feltin, P. de Mierry, B. Beaumont, B. Damilano, N. Grandjean, and P. Gibart: phys. stat. sol. (a) **192**(2) (2002) 394.
23) M. McLaurin and J. S. Speck: phys. stat. sol. RRL **1**(3) (2007) 110.
24) B. Monemar, P. P. Paskov, G. Pozina, C. Hemmingsson, J. P. Bergman, S. Khromov, V. N. Izyumskaya, V. Avrutin, X. Li, H. Morkoş, H. Amano, M. Iwaya, and I. Akasaki: J. Appl. Phys. **115**(5) (2014) 053507.
25) J. Lähnemann, O. Brandt, U. Jahn, C. Pfüller, C. Roder, P. Dogan, F. Grosse, A. Belabbes, F. Bechstedt, A. Trampert, and L. Geelhaar: Phys. Rev. B **86** (2012) 081302.
26) H. Amano, M. Kitoh, K. Hiramatsu, and I. Akasaki: J. Electrochem. Soc. **137**(5) (1990) 1639.
27) U. Kaufmann, M. Kunzer, H. Obloh, M. Maier, C. Manz, A. Ramakrishnan, and B. Santic: Phys. Rev. B **59** (1999) 5561.
28) J. Klootwijk and C. Timmering: In *Proc. IEEE Int. Conf. Microelectronic Test Structures ICMTS* (2004), vol. 17, pp. 247–252.
29) T. Mukai, M. Yamada, and S. Nakamura: Jpn. J. Appl. Phys. **38**(7R) (1999) 3976.
30) T. Mukai: IEEE J. Sel. Top. Quantum Electron. **8**(2) (2002) 264.
31) M. Krames, O. Shchekin, R. Mueller-Mach, G. O. Mueller, L. Zhou, G. Harbers, and M. Craford: J. Display Technol. **3**(2) (2007) 160.
32) Y. Narukawa, M. Ichikawa, D. Sanga, M. Sano, and T. Mukai: J. Phys. D **43**(35) (2010) 354002.
33) B. Galler, M. Sabathil, A. Laubsch, T. Meyer, L. Hoeppel, G. Kraeuter, H. Lugauer, M. Strassburg, M. Peter, A. Biebersdorf, U. Steegmueller, and B. Hahn: phys. stat. sol. (c) **8**(7-8) (2011) 2369.
34) C. Kölper, M. Sabathil, F. Römer, M. Mandl, M. Strassburg, and B. Witzigmann: phys. stat. sol. (a) **209**(11) (2012) 2304.
35) S. Saito, R. Hashimoto, J. Hwang, and S. Nunoue: Appl. Phys. Express **6**(11) (2013) 111004.
36) J.-I. Hwang, R. Hashimoto, S. Saito, and S. Nunoue: Appl. Phys. Express **7**(7) (2014) 071003.
37) R. Hashimoto, J. Hwang, S. Saito, and S. Nunoue: phys. stat. sol. (c) **11**(3-4) (2014) 628.
38) A. Chakraborty, B. A. Haskell, S. Keller, J. S. Speck, S. P. DenBaars, S. Nakamura, and U. K. Mishra: Appl. Phys. Lett. **85**(22) (2004) 5143.
39) S. Jung, Y. Chang, K.-H. Bang, H.-G. Kim, Y.-H. Choi, S.-M. Hwang, and K. H. Baik: Semicond. Sci. Technol. **27**(2) (2012) 024017.
40) K. Okamoto, H. Ohta, D. Nakagawa, M. Sonobe, J. Ichihara, and H. Takasu: Jpn. J. Appl. Phys. **45**(11L) (2006) L1197.
41) M. C. Schmidt, K.-C. Kim, H. Sato, N. Fellows, H. Masui, S. Nakamura, S. P. DenBaars, and J. S. Speck: Jpn. J. Appl. Phys. **46**(2L) (2007) L126.
42) Y.-D. Lin, A. Chakraborty, S. Brinkley, H. C. Kuo, T. Melo, K. Fujito, J. S. Speck, S. P. DenBaars, and S. Nakamura: Appl. Phys. Lett. **94**(26) (2009) 261108.
43) T. Yokogawa and A. Inoue: Proc. SPIE **9003** (2014) 900316.
44) H. Sato, A. Tyagi, H. Zhong, N. Fellows, R. B. Chung, M. Saito, K. Fujito, J. S. Speck, S. P. DenBaars, and S. Nakamura: phys. stat. sol. (RRL) **1**(4) (2007) 162.
45) I. L. Koslow, M. T. Hardy, P. Shan Hsu, P.-Y. Dang, F. Wu, A. Romanov, Y.-R. Wu, E. C. Young, S. Nakamura, J. S. Speck, and S. P. DenBaars: Appl. Phys. Lett. **101**(12) (2012) 121106.
46) Y. Wang, R. Shimma, T. Yamamoto, H. Hayashi, K. Shiohama, K. Kurihara, R. Hasegawa, and K. Ohkawa: J. Crystal Growth **416** (2015) 164.
47) H. Zhong, A. Tyagi, N. N. Fellows, F. Wu, R. B. Chung, M. Saito, K. Fujito, J. S. Speck, S. P. DenBaars, and S. Nakamura: Appl. Phys. Lett. **90**(23) (2007) 233504.
48) Y. Zhao, J. Sonoda, C.-C. Pan, S. Brinkley, I. Koslow, K. Fujito, H. Ohta, S. P. DenBaars, and S. Nakamura: Appl. Phys. Express **3**(10) (2010) 102101.
49) S. Yamamoto, Y. Zhao, C.-C. Pan, R. B. Chung, K. Fujito, J. Sonoda, S. P. DenBaars, and S. Nakamura: Appl. Phys. Express **3**(12) (2010) 122102.
50) I. L. Koslow, J. Sonoda, R. B. Chung, C.-C. Pan, S. Brinkley, H. Ohta, S. Nakamura, and S. P. DenBaars: Jpn. J. Appl. Phys. **49**(8R) (2010) 080203.
51) H. Yamada, K. Iso, M. Saito, H. Masui, K. Fujito, S. P. DenBaars, and S. Nakamura: Appl. Phys. Express **1**(4) (2008) 041101.
52) D. V. Dinh, M. Akhter, S. Presa, G. Kozlowski, D. O'Mahony, P. P. Maaskant, F. Brunner, M. Caliebe, M. Weyers, F. Scholz, B. Corbett, and P. J. Parbrook: phys. stat. sol. (a) **212**(10) (2015) 2196.
53) Q. Dai, Q. Shan, J. Wang, S. Chhajed, J. Cho, E. F. Schubert, M. H. Crawford, D. D. Koleske, M.-H. Kim, and Y. Park: Appl. Phys. Lett. **97**(13) (2010) 133507.
54) J. Nishinaka, M. Funato, and Y. Kawakami: J. Appl. Phys. **112**(3) (2012) 033513.
55) J. Nishinaka, M. Funato, and Y. Kawakami: Appl. Phys. Lett. **106**(8) (2015) 082105.
56) H. Jönen, U. Rossow, H. Bremers, L. Hoffmann, M. Brendel, A. D. Dräger, S. Schwaiger, F. Scholz, J. Thalmair, J. Zweck, and A. Hangleiter: Appl. Phys. Lett. **99**(1) (2011) 011901.
57) S. Hammersley, M. J. Kappers, F. C.-P. Massabuau, S.-L. Sahonta, P. Dawson, R. A. Oliver, and C. J. Humphreys: Appl. Phys. Lett. **107**(13) (2015) 132106.
58) X. Ni, X. Li, J. Lee, S. Liu, V. Avrutin, Ü. Özgür, H. Morkoş, A. Matulionis, T. Paskova, G. Mulholland, and K. R. Evans: Appl. Phys. Lett. **97**(3) (2010) 031110.
59) J. Wang, T. Meisch, D. Heinz, R. Zeller, and F. Scholz: phys. stat. sol. (b) **253**(1) (2016) 174.